A phase and space coherent direct imaging method

Songming Hou[a)]
Mathematics and Statistics, Louisiana Tech University, Ruston, Louisiana 71272

Kai Huang[b)]
Department of Mathematics, Florida International University, Miami, Florida 33199

Knut Solna[c)] and Hongkai Zhao[d)]
Department of Mathematics, University of California at Irvine, Irvine, California 92697

(Received 23 May 2008; revised 20 October 2008; accepted 1 November 2008)

A direct imaging algorithm for point and extended targets is presented. The algorithm is based on a physical factorization of the response matrix of a transducer array. The factorization is used to transform a passive target problem to an active source problem and to extract principal components (tones) in a phase consistent way. The multitone imaging function can superpose multiple tones (spatial diversity/aperture of the array) and frequencies (bandwidth of the probing signal) based on phase coherence. The method is a direct imaging algorithm that is simple and efficient since no forward solver or iteration is needed. Robustness of the algorithm with respect to noise is demonstrated via numerical examples.
 [DOI: 10.1121/1.3035835]

PACS number(s): 43.60.Tj, 43.60.Pt [OAS] Pages: 227–238

I. INTRODUCTION

In reflection seismology, ultrasound imaging in medical applications, detection of defects in nondestructive testing, underground mine detection and target detection using radar or a sonar system, and so on, one seeks to identify the location and shape of some scatterers by sending probing waves and measuring the scattered waves, e.g., using scattering relations. This is in general an ill-posed (nonlinear) inverse problem. Imaging the whole medium using a general inverse problem approach may be too complicated and too expensive to be practical in many applications, for instance, if the imaging domain is large compared to the wavelength. If the background medium is homogeneous and some simple boundary condition is satisfied at the boundary of the target, the inverse problem can be turned into a geometric problem, that is, the problem of determining the shape of the target from the scattered wave field pattern. Using nonlinear optimization approach in this case is still difficult and computationally expensive.

Direct imaging methods, which are not based on nonlinear optimization and hence do not require forward solver or iterations, have attracted a lot of attention recently. If the targets are small compared to the array resolution, the location information can be obtained while the geometry information is not resolved. Several matched filter type of algorithms have been developed for imaging or locating point targets, for example, the multiple signal classification (MUSIC) algorithm.[1–4] Under the assumption of point targets the response matrix (defined in Sec. II) has a simple structure. This structure is used in MUSIC and has also been exploited to focus a wave field on selected scatterers using iterated time reversal.[5–10] The iterated time reversal procedure corresponds to the power method for finding the dominant singular vectors for the response matrix. However, with the point target assumption, physical properties and the geometry of the target are neglected. More importantly an extended target is not a superposition of point targets. For extended targets the response matrix has a more complicated structure. Recently a few MUSIC type of algorithms[11–14] have been developed to image the location and shape of extended targets. A crucial step is to use resolution and noise level based thresholding to determine how many singular vectors of the response matrix span the signal space.

Although the generalized MUSIC algorithm for a single frequency is capable of imaging different types of targets with efficiency, robustness, and accuracy, provided full aperture data are given, for limited aperture the results are typically not very good. Multiple frequencies should be used to complement the lack of spatial aperture.

The MUSIC algorithm is based on the singular value decomposition (SVD) of the response matrix. This decomposition allows for an arbitrary complex phase; therefore, combining different frequencies in a phase coherent way is not direct. In this paper, we propose a multitone imaging algorithm that makes use of coherent information in both phase and space. In particular, we take advantage of phase coherence from multiple frequency data to improve both resolution of robustness of the imaging procedure. The crucial points in our multitone algorithm are (1) physically based factorization of the response matrix that transforms a passive target detection problem to an active source detection problem and (2) a phase coherent imaging function that can superpose multiple tones and multiple frequencies to take advantage of both spatial diversity (aperture) of the array

[a)]Electronic mail: shou@latech.edu
[b)]Electronic mail: khuang@fiu.edu
[c)]Electronic mail: ksolna@math.uci.edu
[d)]Electronic mail: zhao@math.uci.edu

and/or the bandwidth of the probing signal. The proposed method can be parallelized easily since the evaluation of the imaging function at different grids is independent.

The outline of this paper is as follows. In Sec. II we describe how to locate point targets using a method that we call the multitone algorithm. In Sec. III, we generalize the method to imaging of extended targets. Numerical experiments are presented in Sec. IV.

II. RESPONSE MATRIX AND IMAGING POINT TARGETS

Our imaging setup uses an array of transmitters that can send out probing waves into the region of interest and an array of receivers that can record scattered waves. Our measurement data are the response matrix whose elements are the inter-responses between array elements. The arrays can enclose the region of interest (full aperture) or can have partial aperture. For simplicity, we first consider an active array when the array of transmitters and the array of receivers coincide, moreover, time harmonic waves. Assume that there are N transducers, which can function both as a transmitter and as a receiver, and that are located at $\boldsymbol{\xi}_1,\ldots,\boldsymbol{\xi}_N$. The P_{ij} element of the response matrix P is the received signal at transducer j for a probing pulse sent out from transducer i. Assume that there are M point targets located at $\boldsymbol{x}_1,\ldots,\boldsymbol{x}_M$ with reflectivity $\tau_1,\ldots,\tau_M$. The response matrix in the Born approximation has the following simple structure using spatial reciprocity:

$$P_{ij} = \sum_{m=1}^{M} \tau_m G^0(\boldsymbol{x}_m,\boldsymbol{\xi}_i) G^0(\boldsymbol{\xi}_j,\boldsymbol{x}_m)$$

$$= \sum_{m=1}^{M} \tau_m G^0(\boldsymbol{\xi}_i,\boldsymbol{x}_m) G^0(\boldsymbol{\xi}_j,\boldsymbol{x}_m),$$

where $G^0(\boldsymbol{x},\boldsymbol{y})$ is free space Greens function and we suppress the dependence on frequency. In matrix form we have

$$P = \sum_{m=1}^{M} \tau_m \mathbf{g}_m \mathbf{g}_m^T,$$

where

$$\mathbf{g}_m = [G^0(\boldsymbol{\xi}_1,\boldsymbol{x}_m), G^0(\boldsymbol{\xi}_2,\boldsymbol{x}_m), \ldots, G^0(\boldsymbol{\xi}_N,\boldsymbol{x}_m)]^T,$$

$m=1,2,\ldots,M$, are called illumination vectors, each of which corresponds to the received signals at the array for a point source at $\boldsymbol{x}_m$. For an active array, the response matrix is square and symmetric with rank M in general. If the targets are well resolved by the transducer array, i.e., the separation distance between the targets is larger than the resolution of the array, we have that the point spread function

$$\Gamma(\boldsymbol{x}_m,\boldsymbol{x}_{m'}) = \overline{\mathbf{g}}_m^T \mathbf{g}_{m'} \approx 0 \quad \text{if } m \neq m',$$

which means the wave field corresponding to the time reversal of a point source at one target is almost zero at all other targets. Hence $\hat{\mathbf{g}}_m = \mathbf{g}_m / \|\mathbf{g}_m\|$ and its complex conjugate $\overline{\hat{\mathbf{g}}}_m$ can be regarded as the left and right singular vectors for the response matrix P. In general this one to one correspondence does not exit. However, one can show that $\mathbf{g}_m$, $m=1,2,\ldots,M$ still span the signal space of P even if multiple scattering among point targets is present based on the Foldy–Lax formulation.[1]

Remark. Here we assume the simplest model for point scatters. In general, a point scatterer may induce both monopole and dipole for the scattered field. For example, the scattered field for an acoustic point scatterer is the sum of monopole (by contrast in compressibility) and dipole (by contrast in density).[15,16] Our formulation and imaging function only use the monopole component which works for hard scatterers. We should be able to modify our imaging function to take into account dipoles which will be discussed in our future work.

To motivate our imaging algorithm consider first the case with a point source at the mth scatterer location; the vector of observations at the transducer array is then

$$\mathbf{g}(\boldsymbol{x}_m) = [G^0(\boldsymbol{\xi}_1,\boldsymbol{x}_m), G^0(\boldsymbol{\xi}_2,\boldsymbol{x}_m), \ldots, G^0(\boldsymbol{\xi}_N,\boldsymbol{x}_m)]^T.$$

Phase conjugation at the mirror and backpropagation to the imaging domain correspond to forming the imaging function $I_m(\boldsymbol{x}) = \mathbf{g}(\boldsymbol{x}_m)^H \mathbf{g}(\boldsymbol{x})$, where $\boldsymbol{x}$ is a search point in the domain and the superscript H denotes the transpose and complex conjugate. Note that physical *time reversal* corresponds to phase conjugation in frequency domain and then backtransformation to time domain. In the inverse problem setting, although $\boldsymbol{x}_m$ is unknown, an estimate of $\hat{\mathbf{g}}(\boldsymbol{x}_m)$ can be obtained (up to a constant phase) via the SVD of the response matrix. The imaging function will peak at the source location $\boldsymbol{x}_m$ due to phase coherence; $I_m(\boldsymbol{x}_m) = \|\mathbf{g}(\boldsymbol{x}_m)\|^2$. In particular, if we use normalized $\hat{\mathbf{g}}(\boldsymbol{x})$ and $\hat{\mathbf{g}}(\boldsymbol{x}_m)$ in the above imaging function, it is an optimal matched filter.[17–19] Classic Rayleigh resolution theory gives that $I_m(\boldsymbol{x})$ will be supported in the neighborhood of the source-point $\boldsymbol{x}_m$ with a lateral resolution of order $\lambda L/a$. Here $\lambda = c_0/\omega$ is the wavelength, L is the distance from the array to the source, a is the aperture of the array, and c_0 denotes the speed of propagation.

We compute the SVD of the response matrix to extract dominant singular vectors (tones). This matrix factorization corresponds to turning passive targets into imaging sources for the scattered wave. However, the SVD of a matrix is unique up to a complex phase, e.g., if the following is a SVD of P:

$$P = \sum_m \sigma_m \mathbf{u}_m \mathbf{v}_m^H,$$

where $\mathbf{u}_m(\mathbf{v}_m)$ are the unit left (right) singular vectors and σ_m are the singular values of P, then $e^{i\theta_m}\mathbf{u}_m(e^{i\theta_m}\mathbf{v}_m)$ are also left (right) singular vectors for arbitrary θ_m, $m=1,2,\ldots$. To overcome the arbitrary phase in the SVD, we propose the following modified imaging function for each pair of left and right singular vectors $\mathbf{u}_m$ and $\mathbf{v}_m$, which we call a tone of the response matrix:

$$I_m(\boldsymbol{x}) = [\hat{\mathbf{g}}^H(\boldsymbol{x})\mathbf{u}_m][\hat{\mathbf{g}}^H(\boldsymbol{x})\overline{\mathbf{v}}_m].$$

First, this imaging function removes the phase ambiguity of the SVD of the response matrix. Second, for well resolved point targets,

$$I_m(\boldsymbol{x}) = [\hat{\mathbf{g}}^H(\boldsymbol{x})\hat{\mathbf{g}}(\boldsymbol{x}_m)]^2.$$

Note that by "squaring" in this way, instead of using norm square, we maintain the phase information, e.g., the phase information is just linearly doubled. Next, we superpose the dominant tones for the different frequencies to obtain the general form of the multitone imaging function:

$$I^M(\boldsymbol{x}) = \sum_{\omega} \alpha(\omega) \sum_{m=1}^{M^\omega} [\hat{\mathbf{g}}^H(\boldsymbol{x};\omega)\mathbf{u}_m^\omega][\hat{\mathbf{g}}^H(\boldsymbol{x};\omega)\bar{\mathbf{v}}_m^\omega]. \quad (1)$$

We remark that for an active array with the transmitters and receivers coinciding, the response matrix P is complex symmetric and can be factorized as $P = U\Sigma U^T$. The imaging function then becomes

$$I^M(\boldsymbol{x}) = \sum_{\omega} \alpha(\omega) \sum_{m=1}^{M^\omega} [\hat{\mathbf{g}}^H(\boldsymbol{x};\omega)\mathbf{u}_m^\omega]^2. \quad (2)$$

In the general case when the transmitters and receivers do not coincide, e.g., there are s transmitters located at $\boldsymbol{\xi}_1, \ldots, \boldsymbol{\xi}_s$ and there are r receivers located at $\boldsymbol{\eta}_1, \ldots, \boldsymbol{\eta}_r$, the response matrix is of dimension $s \times r$. The ijth element P_{ij} then records the response at jth receiver for a signal sent out from ith transmitter. Define the illumination vector with respect to the receiver array and transmitter array, respectively, as

$$\mathbf{g}_r(\boldsymbol{x}) = [G^0(\boldsymbol{\eta}_1,\boldsymbol{x}), G^0(\boldsymbol{\eta}_2,\boldsymbol{x}), \ldots, G^0(\boldsymbol{\eta}_r,\boldsymbol{x})]^T$$

and

$$\mathbf{g}_s(\boldsymbol{x}) = [G^0(\boldsymbol{\xi}_1,\boldsymbol{x}), G^0(\boldsymbol{\xi}_2,\boldsymbol{x}), \ldots, G^0(\boldsymbol{\xi}_s,\boldsymbol{x})]^T.$$

The response matrix in the Born approximation has the following form in the case of M point targets located at $\boldsymbol{x}_1, \ldots, \boldsymbol{x}_M$ with reflectivity $\tau_1, \ldots, \tau_M$:

$$P = \sum_{m=1}^{M} \tau_m \mathbf{g}_s(\boldsymbol{x}_m)\mathbf{g}_r^T(\boldsymbol{x}_m).$$

Thus, the column and row space of P is spanned by $\mathbf{g}_s(\boldsymbol{x}_m)$ and $\mathbf{g}_r^T(\boldsymbol{x}_m)$, respectively. Accordingly the multitone imaging function is constructed as

$$I^M(\boldsymbol{x}) = \sum_{\omega} \alpha(\omega) \sum_{m=1}^{M^\omega} [\hat{\mathbf{g}}_s^H(\boldsymbol{x};\omega)\mathbf{u}_m^\omega][\hat{\mathbf{g}}_r^H(\boldsymbol{x};\omega)\bar{\mathbf{v}}_m^\omega]. \quad (3)$$

Here $\hat{\mathbf{g}}$ denotes the normalized illumination vector.

The frequency weight function $\alpha(\omega)$ can in principle be chosen to reflect the signal to noise ratio (SNR) of different frequencies. However, here we will not discuss this issue and use a uniform weighting. Note second that M^ω is the number of significant tones which may vary with frequency. If there are M point targets that are well resolved by all the frequencies used, then $M^\omega = M$. In general, e.g., for extended targets, M^ω may be proportional to the resolution of frequency ω.[11,20] In particular, when there is strong noise present, e.g., low SNR, M^ω is an important thresholding (regularization) parameter.[11] An important strength of the multitone algorithm is that it is quite robust with respect to the choice of M^ω. In particular, when the noise level is low, we can choose it to coincide with the smaller dimension of the response matrix. This is not the case for, for instance, the MUSIC algorithm, described below, whose imaging result depends more sensitively on the thresholding.

We summarize by stating that two important features of the multitone imaging algorithm are as follows:

1. The SVD factorization of the response matrix turns a passive target detection problem into an active source detection problem. The principal component (tone) decomposition of the response matrix takes the full array into account simultaneously and extracts dominant information or "tones" via the SVD, giving a robust imaging scheme.
2. The imaging function exploits coherent phase information via superposition of complex tones.

Next, we compare our multitone imaging algorithm with two other popular imaging algorithms. For simplicity we discuss the active array case.

1. MUSIC. The MUSIC imaging function[4] is based on the projection to the signal space spanned by dominant singular vectors, which is equivalent to the following quantity:

$$\sum_{m=1}^{M} |\hat{\mathbf{g}}^H(\boldsymbol{x})\mathbf{u}_m|^2,$$

where M is the dimension of the signal space that is determined according to the resolution and/or the SNR analysis.[11,20] However, phase information is lost after projection and hence it is difficult to superpose multiple frequencies based on phase coherence. Thus, travel time information is not effectively utilized in this implementation of the MUSIC imaging functional.
2. Kirchhoff migration. The Kirchhoff migration is a time domain method which exploits travel time information between pairs of transducers. After Fourier transform it can be approximated in frequency domain[21] by the following:

$$\tilde{\mathbf{g}}^H(\boldsymbol{x})P\bar{\tilde{\mathbf{g}}}(\boldsymbol{x}) = \tilde{\mathbf{g}}^H(\boldsymbol{x})\left[\sum_{m=1}^{N} \sigma_m \mathbf{u}_m \mathbf{v}_m^H\right]\overline{\tilde{\mathbf{g}}(\boldsymbol{x})},$$

where $\tilde{\mathbf{g}}(\boldsymbol{x})$ is Green's function without the spatial decaying factor $(1/\|\boldsymbol{x}\|)$ and N is the number of transducers. The above formula is similar to Eq. (1) for each frequency except the following two main differences: (1) our imaging function does not contain the weighting by the singular values and (2) our imaging function introduces a thresholding/regularization based on resolution and/or SNR. These two differences mean that the multitone imaging algorithm only separates signal space from noise space and treats all dominant signals, i.e., dominant singular vectors, equally. The motivation comes from the following observations: a point target partially blocked by other targets will contribute a singular vector with smaller singular values. So our multitone imaging function will increase the visibility of partially blocked targets compared to Kirchhoff migration, as shown in Figs. 2 and 3 in Sec. IV A. Also an extended target is not

a superposition of point targets. For example, it is illustrated in Ref. 11 that each singular vector does not correspond to a point on the boundary of an extended target. The geometry of the boundary is embedded in the signal space spanned by the dominant singular vectors collectively. Hence the multitone imaging function will serve to give a uniform illumination of the visible parts of the boundary.

In summary our multitone imaging algorithm takes advantages of both approaches in a natural way. Like MUSIC, our algorithm is based on the SVD of the response matrix and a resolution and/or SNR based thresholding to extract principal components (tones) from the full array information. The principal components are used collectively and in a uniform weighting situation. This is particularly important for imaging extended targets. The response matrix for an extended target can have many principal components.[12,16,22–26] The collection of all these principal components contains information about the extended target. On the other hand, instead of using a projection operator as in MUSIC, we use a propagation operator as in the Kirchhoff method which maintains coherent phase information and allows linear superposition of different tones (components) and multiple frequencies. Only at locations with strong scattering are phases of different tones and different frequencies in our imaging function coherent. Like in the Kirchhoff method travel time information is thus utilized in our imaging function. Our approach is based on gaining robustness via using the SVD of the response matrix to extract coherent information and is extremely simple to implement. We remark that other recent approaches like the coherent interferometric (CINT) method[21] aim at extracting information via carefully screened cross correlation computations of the observations. This approach has been shown to work well in a strongly heterogeneous environment but is less direct in its implementation.

III. EXTENDED TARGETS

A. Dirichlet boundary condition

We consider the situation with an extended target. First, let us assume a Dirichlet boundary condition for the target, i.e., a sound-soft target. Let Ω denote the target and Ω^c the exterior of the target. Let $G_\Omega(\boldsymbol{x},\boldsymbol{y})$ be associated Green's function that solves

$$\Delta G_\Omega(\boldsymbol{x}) + k^2 G_\Omega(\boldsymbol{x}) = \delta(\boldsymbol{x}-\boldsymbol{y}), \quad \boldsymbol{x},\boldsymbol{y} \in \Omega^c \subset R^m,$$

$$G_\Omega(\boldsymbol{x},\boldsymbol{y}) = 0, \quad \boldsymbol{x} \in \partial\Omega,$$

and a far field radiation boundary condition. The scattered field at transducer $\boldsymbol{\xi}_j$ corresponding to a point source at $\boldsymbol{\xi}_i$ follows from Greens formula and is

$$P_{ij} = \int_{\partial\Omega} G^0(\boldsymbol{\xi}_i,\boldsymbol{y}) \frac{\partial G_\Omega(\boldsymbol{\xi}_j,\boldsymbol{y})}{\partial \nu} d\boldsymbol{y},$$

where G^0 is free space Green's function. A physical interpretation is that the source of the scattered wave field is a weighted superposition of monopoles at the boundary. The response matrix can be written as

$$P = \int_{\partial\Omega} \mathbf{g}(\boldsymbol{y}) \left[\frac{\partial \mathbf{g}_\Omega(\boldsymbol{y})}{\partial \nu} \right]^T d\boldsymbol{y}, \tag{4}$$

where $\mathbf{g}(\boldsymbol{y})$ is the illumination vector for the homogeneous background, which is known, and $\mathbf{g}_\Omega(\boldsymbol{y})$ is the illumination vector

$$g_\Omega(\boldsymbol{y}) = [G_\Omega(\boldsymbol{\xi}_1,\boldsymbol{y}), \ldots, G_\Omega(\boldsymbol{\xi}_N,\boldsymbol{y})]^T,$$

which is unknown.

Equation (4) gives a factorization of the response matrix that separates the known and unknown components. Thus, the response matrix is superposed from illumination vector $\mathbf{g}(\boldsymbol{y})$, where $\boldsymbol{y}$ belongs to the illuminated parts of the boundary, e.g., where $\partial_{\mathbf{g}\Omega}(\boldsymbol{y})/\partial_\nu$ is not small. Therefore, we apply SVD to the response matrix to extract the singular vectors $\mathbf{u}_m(\mathbf{v}_m)$ and then use the imaging functions (2) for symmetric active array and (3) if the transmitter array and receiver array are different. This imaging function will peak at the well illuminated parts of the boundary. Physically, the peak can be explained by the fact that the boundary acts as a source for the scattered field; thus also, iterated time reversal, i.e., power method for finding singular vectors, will give focusing on the boundary. The thresholding strategy for extended targets introduced in Ref. 11 can be used to determine the thresholding parameter by an optimal cutoff.

We remark that the unknown weight function (illumination strength) for the monopoles at the target boundary, $\partial_{\mathbf{g}\Omega}(\boldsymbol{y})/\partial_\nu$, is not uniform in general due to geometry of the target, such as singularities and concavity of the boundary, and/or the array configuration, such as illumination angles and partial aperture. Locations on the boundary with stronger wave field, i.e. better illuminated by the source, have more weights. These factors will be reflected by the magnitude of singular values for different singular vectors. In our multitone algorithm each principal component will be given an equal weight as long as its corresponding singular value is above the noise threshold. That is why our imaging function gives a fairly uniform intensity on the well illuminated boundary. This is an important aspect of our approach: by taking out the scaling of the tones by the singular values we focus on the geometrical aspects of the extended scatterer and compensate for differences in relative illumination strength. Thus differential parts of the boundary are imaged with a similar fidelity.

B. Neumann boundary condition

For a sound-hard target, with a Neumann boundary condition for the extended target the response matrix has the form

$$P = -\int_{\partial\Omega} \left[\frac{\partial \mathbf{g}(\boldsymbol{y})}{\partial \nu} \right] \mathbf{g}_\Omega^T(\boldsymbol{y}) d\boldsymbol{y}.$$

In other words, the source of the scattered wave field is an (unknown) weighted superposition of dipoles $\partial \mathbf{g}(\boldsymbol{y})/\partial\nu$ at the boundary. Therefore, the normal direction is part of the un-

known in the imaging function. As is done in Ref. 11 we will incorporate a direction search in our imaging function, e.g., among a fixed collection of discretized directions, μ_j, $j=1,2,\ldots$, we maximize the imaging function among these directions at a searching point $\boldsymbol{x}$. Our multitone imaging function is then in the general case:

$$I^M(\boldsymbol{x}) = \max_j \left| \sum_{\omega} \alpha(\omega) \sum_{m=1}^{M^\omega} \left[\frac{\partial \hat{\mathbf{g}}_s^H(\boldsymbol{x};\omega)}{\partial \nu_j} \mathbf{u}_m^\omega \right] \left[\frac{\partial \hat{\mathbf{g}}_r^H(\boldsymbol{x};\omega)}{\partial \nu_j} \bar{\mathbf{v}}_m^\omega \right] \right|.$$

C. Limited or synthetic aperture

For single frequency and full aperture the MUSIC algorithm typically works better than multitone. However, for limited aperture or synthetic aperture with multiple frequency data MUSIC may fail while multitone can work well. We demonstrate below that the multitone algorithm works well also in a case with limited or synthetic aperture.

D. Far field data

In Sec. II the response matrix is defined in terms of near field data, with the sources and receivers in near field. In some applications, the measurement data are far field data, that is, the incident field is essentially a plane wave and the far field pattern of the scattered field is recorded.

We now discuss briefly the case for far field data. For Dirichlet boundary condition, the element of the response matrix P_{ij} corresponds to the far field pattern of the scattered field in the jth direction due to an incident wave coming from the ith direction:

$$P_{ij} = u_\infty(\hat{\boldsymbol{\theta}}_j;\hat{\boldsymbol{\theta}}_j) = \beta \int_{\partial\Omega} \frac{\partial u}{\partial \nu}(\boldsymbol{y};\hat{\boldsymbol{\theta}}_i) e^{-ik\hat{\boldsymbol{\theta}}_j\cdot\boldsymbol{y}} d\boldsymbol{y},$$

where the total field u is due to incident plane wave coming from the direction $\hat{\boldsymbol{\theta}}_i$, where $\beta=-1/4\pi$ for three dimensions and $\beta=-e^{i\pi/4}/\sqrt{8\pi|k|}$ for two dimensions.

In matrix form

$$P = \beta \int_{\partial\Omega} \frac{\partial \vec{u}}{\partial \nu} \hat{\mathbf{g}}^H(\boldsymbol{y}) d\boldsymbol{y}, \tag{5}$$

where

$$\hat{\mathbf{g}}(\boldsymbol{y}) = [e^{ik\hat{\boldsymbol{\theta}}_1\cdot\boldsymbol{y}}, \ldots, e^{ik\hat{\boldsymbol{\theta}}_n\cdot\boldsymbol{y}}]^T,$$

and $\vec{u}$ is the vector of total fields corresponding to the incident plane waves from $\hat{\boldsymbol{\theta}}_1,\ldots,\hat{\boldsymbol{\theta}}_n$. Equation (5) gives a physical factorization of the scattered field into known and unknown parts. The far field pattern is a superposition of the far field patterns of point sources located on the boundary of the target; however, we do not know the weight function which depends on the total field. In other words, the scattering at the target boundary acts as "sources" for the scattered field. In this far field setup, it is natural to use $\hat{\mathbf{g}}(\boldsymbol{y})$ as the illumination vector as discussed in Ref. 12. The signal space of the response matrix should be well approximated by the span of the illumination vectors $\hat{\mathbf{g}}(\boldsymbol{y})$ with $\boldsymbol{y}$ on the well-illuminated part of the boundary of the targets. Hence, we only need to change the form of illumination vectors in the multitone imaging function. Neumann type of boundary conditions can also be dealt in a similar fashion as in the case with near field data. See Ref. 12 for more details.

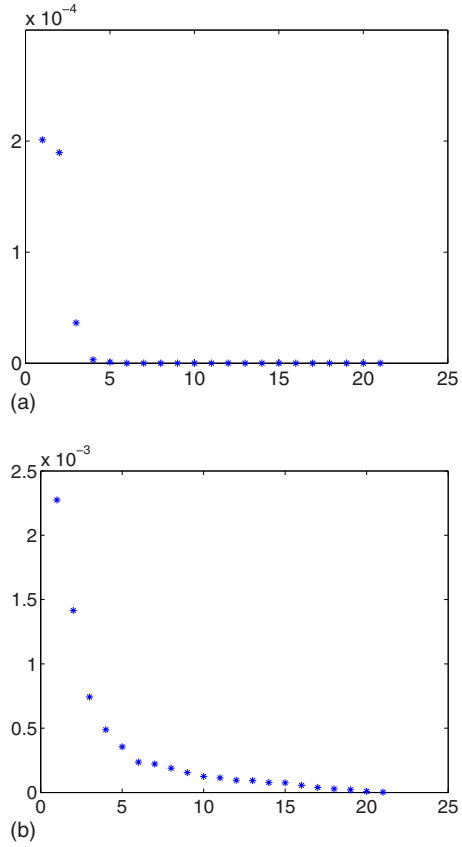

FIG. 1. (Color online) SVD pattern of the response matrix.

IV. NUMERICAL EXPERIMENTS

A. Point targets

First we show a few examples for point targets, targets that are small compared to the resolution of the array. The examples are two dimensional (2D) experiments and simulations.

In the first numerical test, there are three targets with a range of 30–40λ (central wavelength). The linear active array is located at the left side and is composed of 21 transducers that are half wavelength apart, i.e., the aperture is 10λ. The three targets are of size 0.5λ each. We tested this setup in both homogeneous and random media. The weakly heterogeneous medium has a 5% standard deviation and the correlation length is $O(\lambda)$. Finite difference method is used to solve the Helmholtz equation with perfectly matched layer (PML) technique[27] for 21 frequencies that are equally distributed between 0.9λ and 1.1λ with equal weight. The size of grid in numerical scheme is $\lambda/10$ in the 2D rectangle domain. The star shows the true location of targets.

Figure 1 shows the SVD pattern for a fixed frequency (0.9λ) for these two cases. In the homogeneous medium, there are only three dominant singular values. However, the three singular vectors may not have a one to one correspondence to the illumination vector of the three targets due to

multiple scattering among the targets. In particular, the reflected wave from the rear scatterer will be mixed with the reflection of the two front ones.

The numerical data used for imaging targets in heterogeneous medium are the scattered wavefield by the target and the background heterogeneous medium, i.e., the difference of the two wavefields corresponding to the medium with targets and the homogeneous medium, respectively. The goal is to image dominant scatterers/targets without imaging or knowing the details of the background medium, which is very desirable in many practical applications. The situation is also more difficult than using the difference data, i.e., measuring the difference of the two wavefields corresponding to the medium with targets and the same medium without targets, respectively. Figures 2 and 3 show the imaging results using multitone imaging algorithm using different number of frequencies and different number of leading singular vectors. It shows clearly that

- superposition of coherent phases from multiple frequencies improves range resolution;
- using the leading three singular vectors (the best SNR thresholding) produces the best results; however, the imaging result is not very sensitive to thresholding; and
- the partially blocked target has a better visibility compared to the Kirchhoff migration for the reason discussed in Sec. II.

As shown in Fig. 1, the SVD pattern is more complicated in random medium due to multipathing. Figure 4 shows the imaging results using the multitone imaging algorithm, which demonstrates the following:

- The location information of three point targets is not included in the first three singular vectors.
- Involving more singular vectors, even without thresholding, works well since only strong scattering at targets is superposed coherently (in phase) across different frequencies.
- Again the partially blocked target has a better visibility compared to the Kirchhoff migration.

Finally we test our algorithms on real experimental data. The data were kindly provided by Daniel D. Stancil and his group at Carnegie Mellon University. In their experimental setup, transmit array A and receive array B are used, as shown in Fig. 5. The locations of transmitters and receivers are different. The measurements were taken at 201 frequency points ranging from 4 to 6 GHz. An absorbing wall is located behind the test scenario.

Figure 6 shows imaging using data with different numbers of targets. The stars in each figure are the true locations of targets.

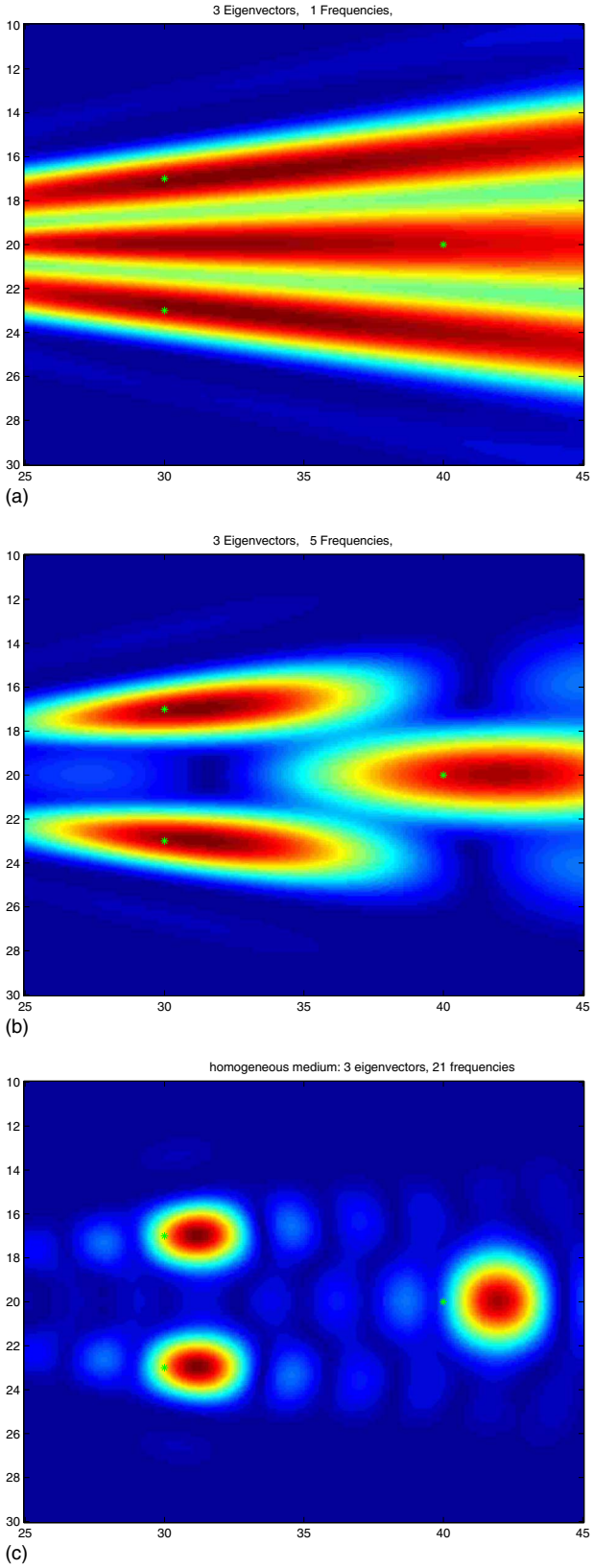

FIG. 2. (Color online) Imaging point targets in homogeneous medium. Multitone algorithm using 3 leading singular vectors and (a) 1 frequency, (b) 5 frequencies, and (c) 21 frequencies.

B. Extended targets

In this section we test our multitone imaging algorithm on extended targets with full aperture, limited aperture, and synthetic aperture using near and far field data. All near field data are simulated by solving the Helmholtz equation using finite difference method with PML (Ref. 27) boundary condition. For inverse problems, the forward solver is not required to be very accurate, we did not use any special treatment at the target boundary, i.e., the standard five point

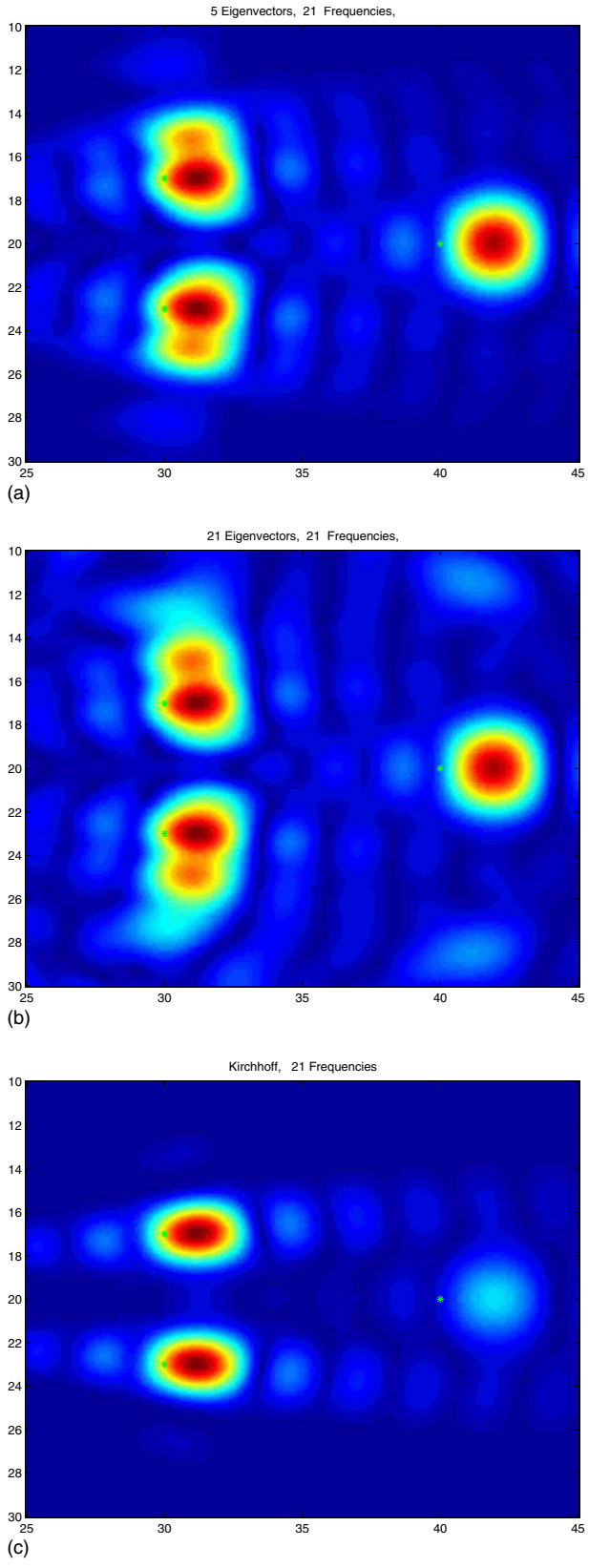

FIG. 3. (Color online) Imaging point targets in homogeneous medium. Multitone algorithm using 21 frequencies and (a) 5 leading singular vectors, (b) 21 singular vectors, and (c) Kirchhoff algorithm using 21 frequencies.

stencil for centered difference is used at every grid node. Far field data are generated using a boundary integral method.[12,28] The simulations are in 2D.

We give two examples with full or limited aperture near field data, two examples with synthetic aperture near field data, one example with full aperture far field data, one example where sources and receivers do not coincide, and finally, one example with limited aperture far field data. For all near field experiments, the transducers are about $200h$ (200 grid cells) away from the target and the forward data are again generated using a finite difference method with the PML technique.[27] The multiplicative noise is modeled by $P_{\text{noisy}}(i,j)=\text{Re}(P(i,j))a+\text{Im}(P(i,j))b$, where a and b are uniformly distributed in $[1-c,1+c]$, where c is 10%. The random medium or *clutter* is modeled as follows: The index of refraction $n(x)$ is a Gaussian with mean one and standard deviation 10% and the correlation length is $10h$, which is comparable but less than the wavelength.

Figure 7 shows imaging of a single extended target in a homogeneous medium. The full circular active array has 80 transducers surrounding the target. When a single frequency is used the corresponding wavelength is $\lambda=16h$. When three frequencies are used, they correspond to wavelengths, $\lambda=16h,24h,32h$. The target is about $200h$ away from the array and its size is about $80-100h$. In this test, no thresholding is used in the multitone imaging function. It is clear that phases across different frequencies are superposed coherently at the boundary only, where strong scattering happens. Figure 8 shows imaging of the same target with limited aperture data. Only half of the circular array from the bottom is used.

Figure 9 shows the imaging of a sound-hard (Neumann boundary condition) target with full aperture circular array (80 transducers). The array is about $200h$ from the center of the target. Six equally spaced frequencies are used, with lowest frequency $\lambda=32h$ and highest frequency $\lambda=16h$.

We next test with synthetic aperture. We use the following implementation of synthetic aperture. Let P be an 80-by-80 response matrix corresponding to an active circular array with full aperture (as above), and $P_n=Q(n:n+19,n:n+19)$, where $n=1,11,21,\ldots,61$, then the P_n's are the 20-by-20 response matrices with limited aperture and a partial overlap. We use P_n at the same six frequencies as above.

Figure 10 shows the multitone imaging function with synthetic aperture data for a sound-soft (Dirichlet boundary condition) object. The top one is the result for homogeneous medium with clean simulated data. For the middle one, 10% multiplicative noise is added to the data. The bottom one shows imaging in a random medium with 10% standard deviation. The correlation length is about a wavelength.

In contrast, the MUSIC algorithm does not provide a good imaging function for limited/synthetic aperture data. Figure 11 shows the result using the MUSIC algorithm with synthetic aperture data. The kite shape is not clear.

Finally we test the multitone imaging algorithm using far field data. The only change made is in the form of the illumination vector, i.e., using the far field pattern of Green's function. Figure 12 shows the multitone imaging function for far field data with clean simulated data (left) and with 100% multiplicative noise added to the simulated data (right).

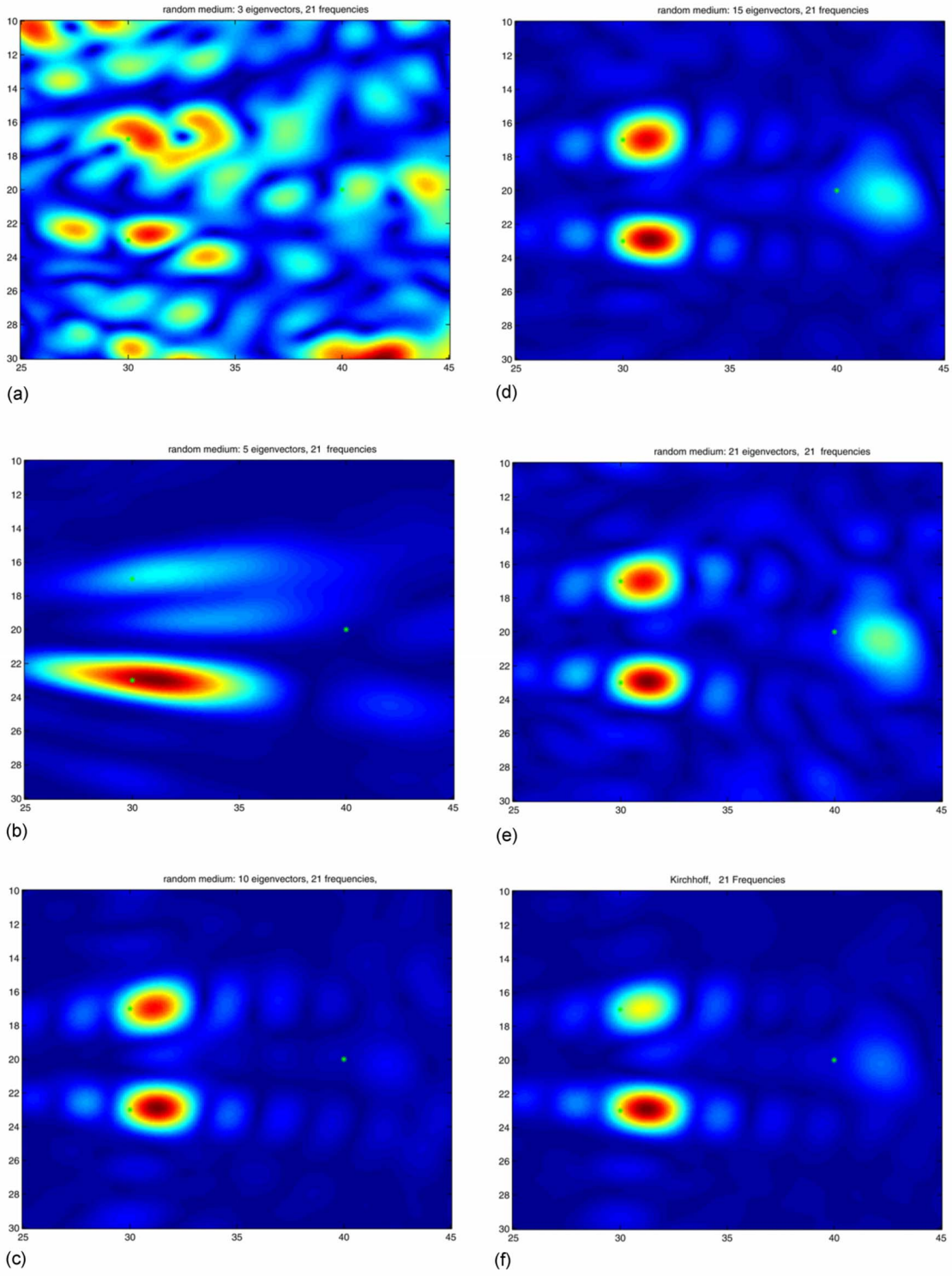

FIG. 4. (Color online) Imaging point targets in random medium. Multitone algorithm using 21 frequencies and (a) 3, (b) 5, (c) 10, (d) 15, and (e) 21 singular vectors, and (f) Kirchhoff algorithm using 21 frequencies.

Three wave numbers are used, $k=5,6,7$, so that the target sizes are on the scale of the wavelength. The forward data are here generated using the boundary integral method. In this case 32 plane incident waves are used and the far field data are collected at the same 32 directions.

We remark that the thresholding strategy discussed in Ref. 11 is used for all the above examples of extended targets except the first one. In principle, with thresholding only the first few dominant singular vectors are used in the multitone imaging function. This is known to be robust as long as the leading singular values are well separated from the remainder. However, in our tests the results are not very sensitive to the thresholding, which means that the multitone imaging function is already quite robust and is easier to use in prac-

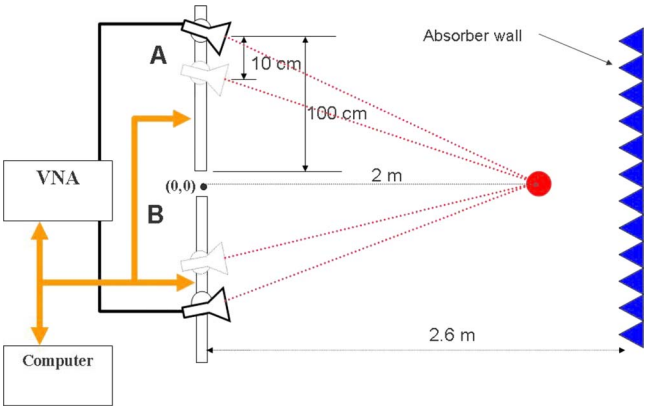

FIG. 5. (Color online) CMU experiment setup.

tice. Thus we also expect that our imaging results are robust with respect to numerical errors and artifacts by our numerical scheme that generates the data.

In the last set of tests, we show imaging with arrays that have transmitters different from receivers, or plane wave incident angles different from far field data angles. Figure 13 shows the multitone imaging function using wave numbers $k=5,6,7$ for far field data with plane wave incident from the right (16 directions) and far field pattern recorded on the left (16 directions). Dirichlet boundary condition is used.

Again, for limited aperture only part of the boundary that is well illuminated is seen in the imaging function. Figure 14 shows the multitone imaging function using wave numbers $k=5,6,7$ for far field data with limited aperture, that is, only plane waves in a 180 deg angle are used (16 directions) and the far field data within the same angle are recorded. Only the part of the kite boundary that is well illuminated by the array can be observed in the imaging function.

V. CONCLUSIONS

We propose a direct imaging algorithm, the multitone method. The algorithm is simple and efficient because no forward solver or iteration is needed. This method provides a framework for balancing spatial diversity via the SVD with

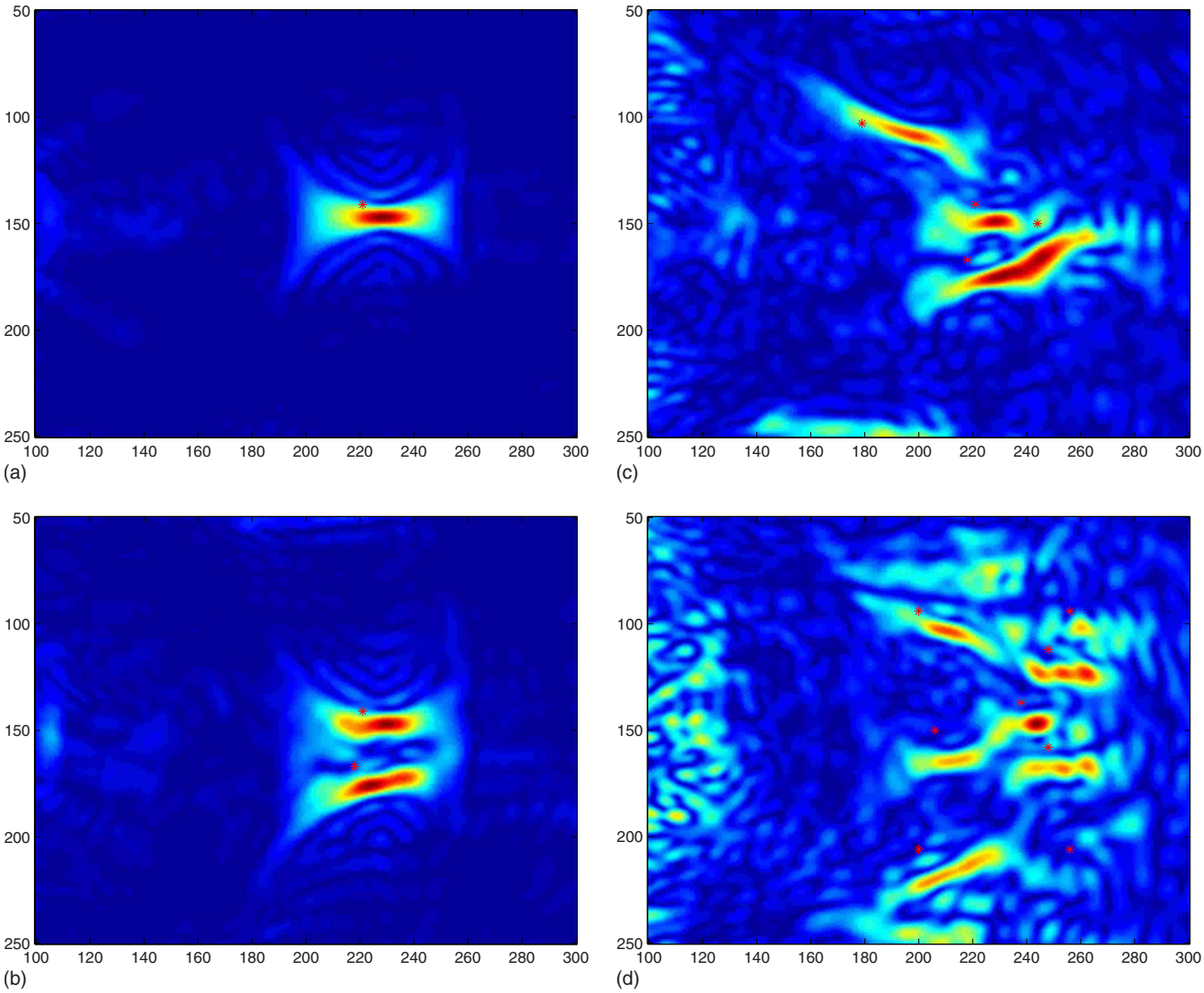

FIG. 6. (Color online) CMU experiment data imaging: (a) one target, (b) two targets, (c) four targets, and (d) eight targets.

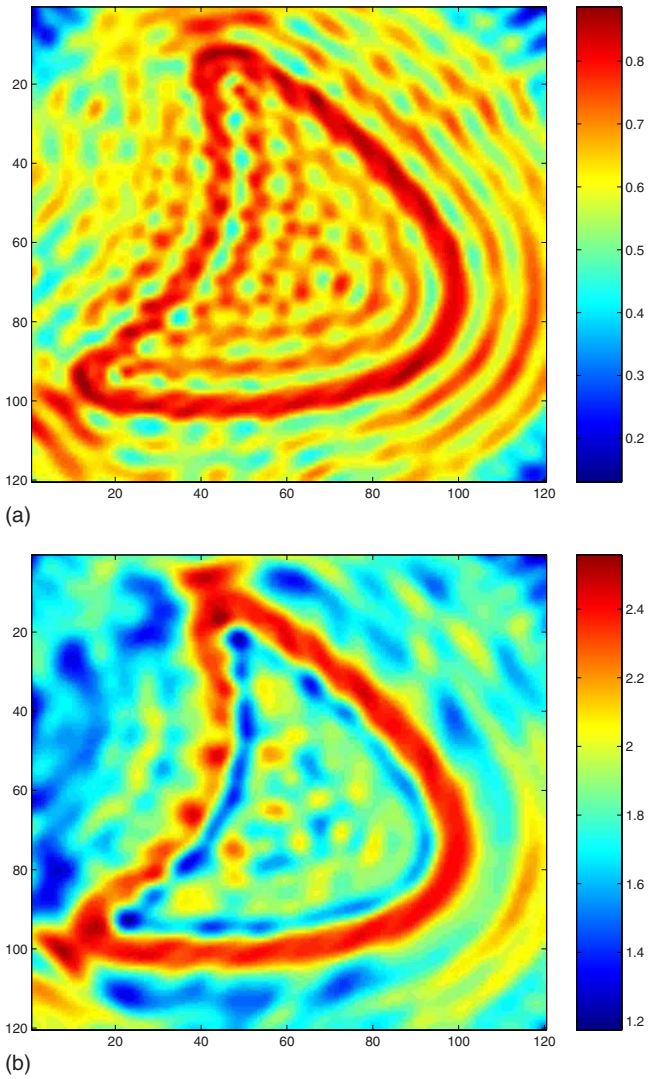

FIG. 7. (Color online) Multitone algorithm using full aperture data with one frequency (left) and three frequencies (right).

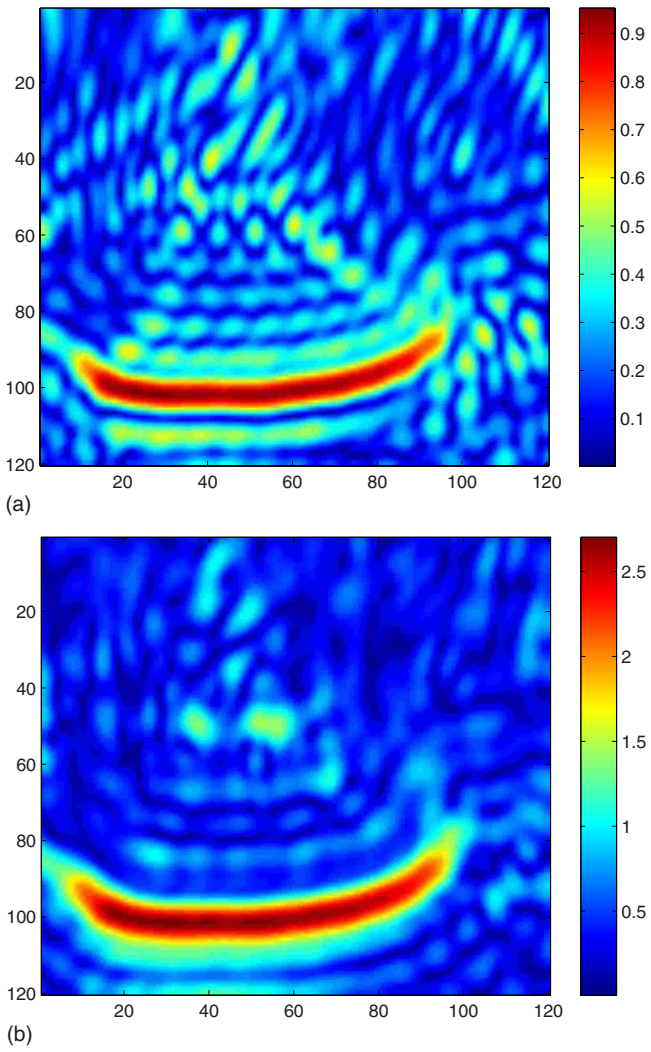

FIG. 8. (Color online) Multitone algorithm using limited aperture data (half of the circular array from the bottom) with one frequency (left) and three frequencies (right).

frequency diversity via superposition of coherent phases. By taking advantage of phase coherence of multiple frequencies, the imaging is enhanced and is robust with respect to noise. The algorithm can deal with limited or synthetic aperture data naturally as well as with different material properties and different types of illuminations and measurements.

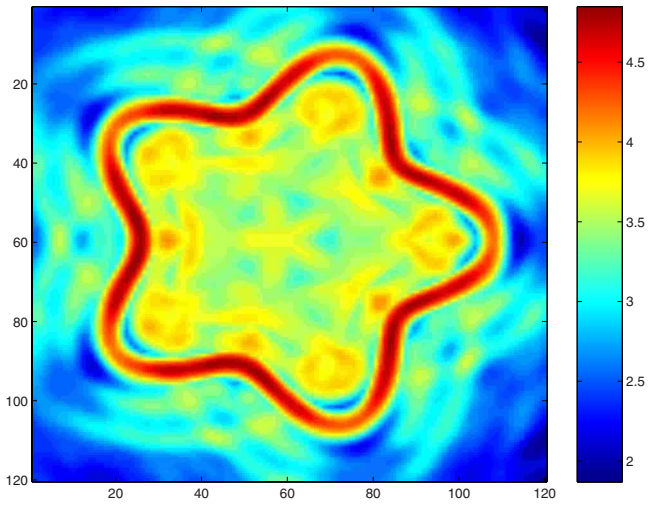

FIG. 9. (Color online) Imaging of extended target with Neumann boundary condition and full aperture using the multitone algorithm with six frequencies.

ACKNOWLEDGMENTS

We would like to thank our collaborators at Carnegie Mellon University, J. M. F. Moura, D. Stancil, and J. Zhu for providing us the experimental data. The research is partially supported by ONR Grant No. N00014-02-1-0090, DARPA Grant No. N00014-02-1-0603, NSF Grant No. 0307011, the Sloan Foundation, and Louisiana Board of Regents RCS Grant No. LEQSF(2008-11)-RD-A-18.

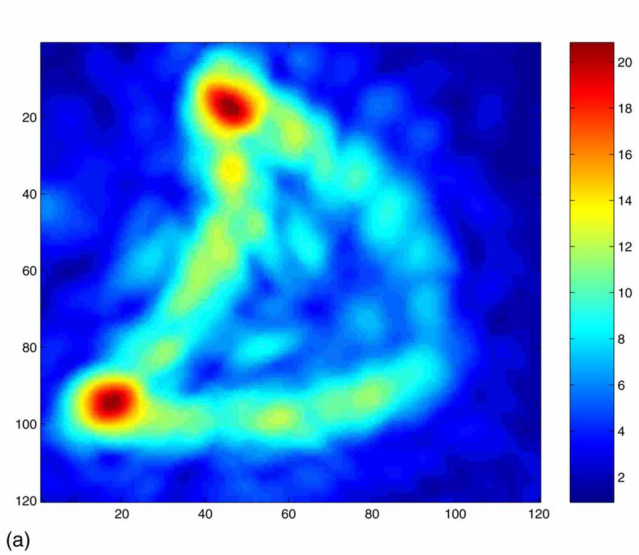

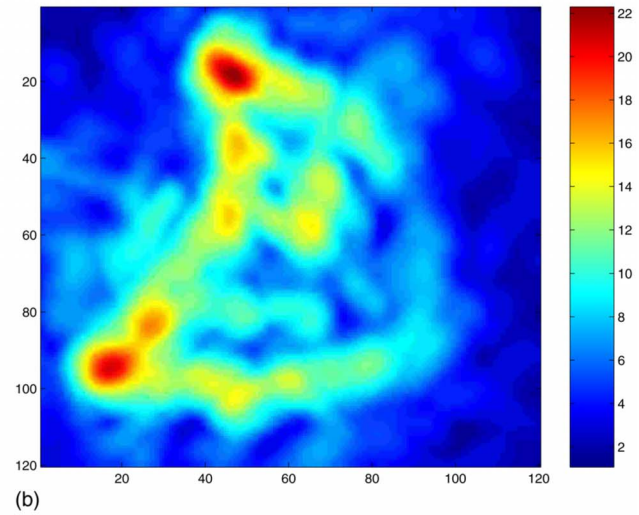

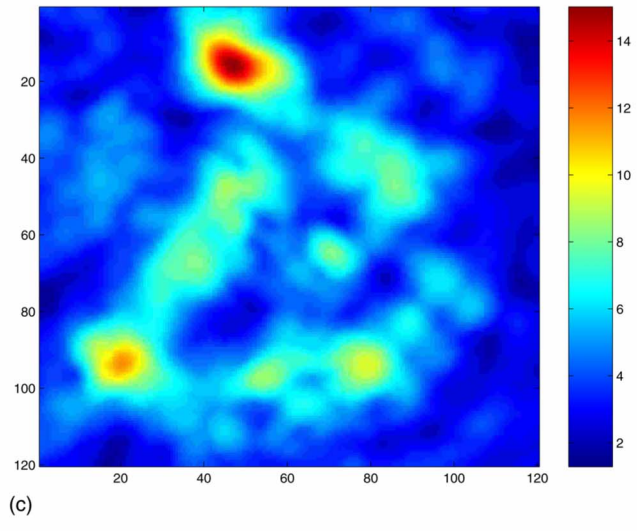

FIG. 10. (Color online) Synthetic aperture multitone imaging for a kite shape with clean data on the top, 10% multiplicative noise in the middle, and 10% random medium fluctuations on the bottom.

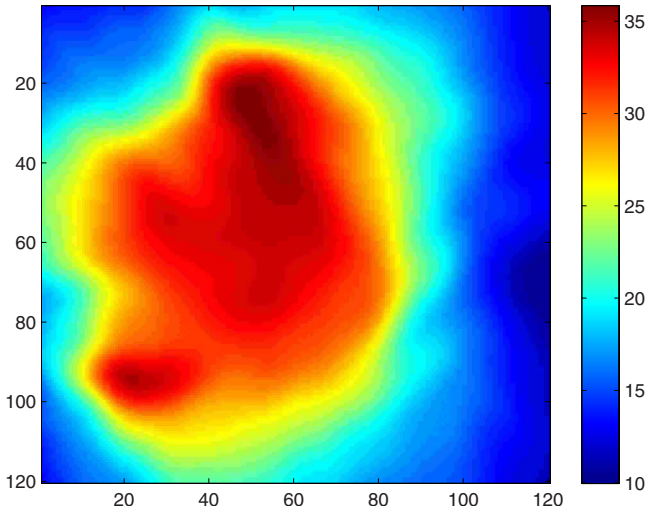

FIG. 11. (Color online) MUSIC imaging function for a kite shape with clean synthetic aperture data. The result is poor.

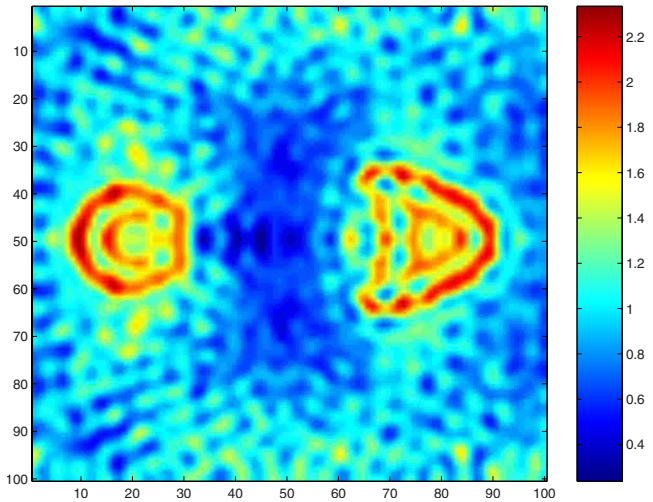

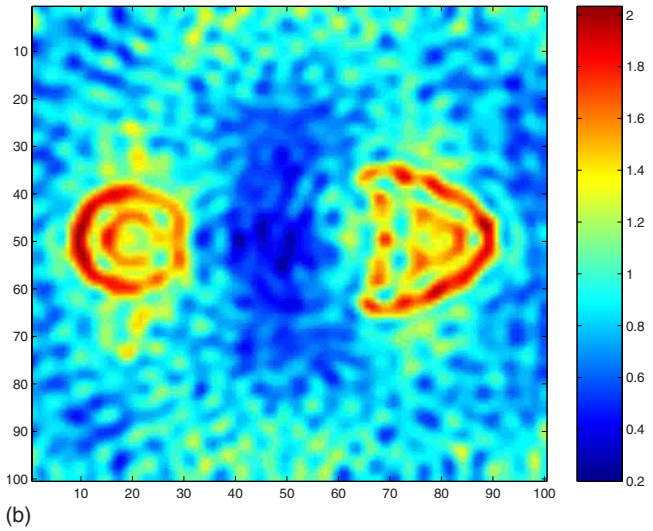

FIG. 12. (Color online) Multitone imaging for a kite shape and a circular shape using far field data with 100% multiplicative noise.

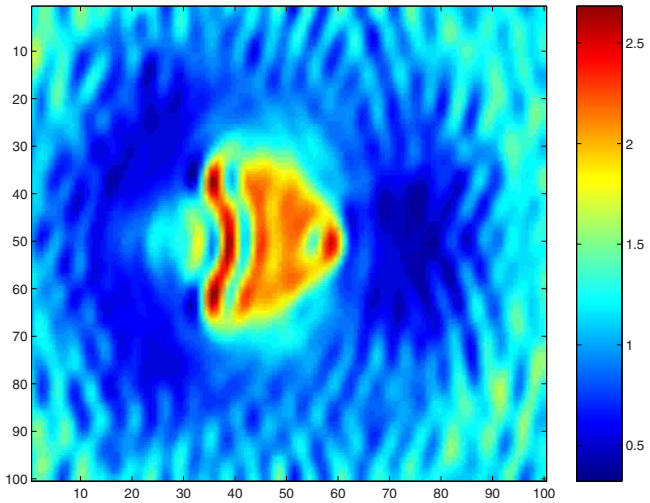

FIG. 13. (Color online) Multitone imaging for a kite shape with incident plane wave directions different from recorded far field data directions.

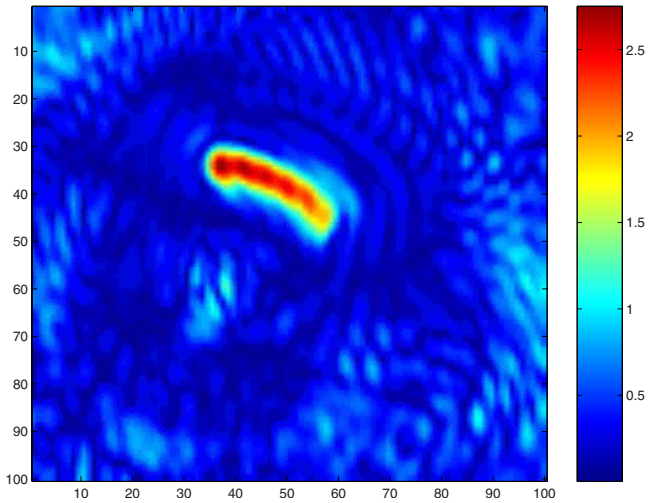

FIG. 14. (Color online) Multitone imaging with limited aperture far-field data.

[1]F. K. Gruber, E. A. Marengo, and A. J. Devaney, "Time-reversal imaging with multiple signal classification considering multiple scattering between the targets," J. Acoust. Soc. Am. **115**, 3042–3047 (2004).
[2]E. Kerbrat, C. Prada, and M. Fink, "Imaging in the presence of grain noise using the decomposition of the time reversal operator," J. Acoust. Soc. Am. **113**, 1230–1240 (2003).
[3]C. Prada and J.-L. Thomas, "Experimental subwavelength localization of scatterers by decomposition of the time reversal operator interpreted as a covariance matrix," J. Acoust. Soc. Am. **114**, 235–243 (2003).
[4]R. O. Schmidt, "Multiple emitter location and signal parameter estimation," IEEE Trans. Antennas Propag. **34**, 276–280 (1986).
[5]E. Kerbrat, C. Prada, D. Cassereau, and M. Fink, "Ultrasonic nondestructive testing of scattering media using the decomposition of the time reversal operator," IEEE Trans. Ultrason. Ferroelectr. Freq. Control **49**, 1103–1113 (2002).
[6]J.-G. Minonzio, C. Prada, D. Chambers, D. Clorennec, and M. Fink, "Characterization of subwavelength elastic cylinders with the decomposition of the time-reversal operator: Theory and experiment," J. Acoust. Soc. Am. **117**, 789–798 (2005).
[7]G. Montaldo, M. Tanter, and M. Fink, "Real time inverse filter focusing by iterative time reversal," J. Acoust. Soc. Am. **115**, 768–775 (2004).
[8]G. Montaldo, M. Tanter, and M. Fink, "Revisiting iterative time reversal processing: Application to detection of multiple targets," J. Acoust. Soc. Am. **115**, 776–784 (2004).
[9]C. Prada, S. Manneville, D. Spoliansky, and M. Fink, "Decomposition of the time reversal operator: Detection and selective focusing on two scatterers," J. Acoust. Soc. Am. **99**, 2067–2076 (1996).
[10]C. Prada, J.-L. Thomas, and M. Fink, "The iterative time reversal process: Analysis of the convergence," J. Acoust. Soc. Am. **97**, 62–71 (1995).
[11]S. Hou, K. Solna, and H. Zhao, "A direct imaging algorithm for extended targets," Inverse Probl. **22**, 1151–1178 (2006).
[12]S. Hou, K. Solna, and H. Zhao, "A direct imaging method using far field data," Inverse Probl. **23**, 1533–1546 (2007).
[13]E. Marengo, F. Gruber, and F. Simonetti, "Time-reversal music imaging of extended targets," IEEE Trans. Image Process. **16**, 1967–1984 (2007).
[14]E. Marengo, R. Hernandez, and H. Lev-Ari, "Intensity-only signal-subspace-based imaging," J. Opt. Soc. Am. A **24**, 3619–3635 (2007).
[15]P. M. Morse and K. U. Ingard, *Theoretical Acoustics* (Princeton University Press, Princeton, NJ, 1968).
[16]D. Chambers and A. Gautesen, "Time reversal for a single spherical scatter," J. Acoust. Soc. Am. **109**, 2616–2614 (2001).
[17]D. H. Chambers, J. V. Candy, S. K. Lehman, J. S. Kallman, A. J. Poggio, and A. W. Meyer, "Time reversal and the spatio-temporal matched filter (L)," J. Acoust. Soc. Am. **116**, 1348–1350 (2004).
[18]M. Tanter, J.-F. Aubry, J. Gerber, J.-L. Thomas, and M. Fink, "Optimal focusing by spatio-temporal inverse filter. I. Basic principles," J. Acoust. Soc. Am. **110**, 37–47 (2001).
[19]M. Tanter, J.-F. Aubry, J. Gerber, J.-L. Thomas, and M. Fink, "Optimal focusing by spatio-temporal inverse filter. II. Experiments. Application to focusing through absorbing and reverberating media," J. Acoust. Soc. Am. **110**, 48–58 (2001).
[20]M. Tanter, J.-L. Thomas, and M. Fink, "Time reversal and the inverse filter," J. Acoust. Soc. Am. **108**, 223–234 (2000).
[21]L. Borcea, G. Papanicolaou, and C. Tsogka, "Coherent interferometric imaging," Geophysics **71**, S1165–S1175 (2006).
[22]D. H. Chambers and J. G. Berryman, "Analysis of the time-reversal operator for a small spherical scatterer in an electromagnetic field," IEEE Trans. Antennas Propag. **52**, 1729–1738 (2004).
[23]D. H. Chambers and J. G. Berryman, "Time-reversal analysis for scatterer characterization," Phys. Rev. Lett. **92**, 023902 (2004).
[24]D. H. Chambers, "Analysis of the time-reversal operator for scatterers of finite size," J. Acoust. Soc. Am. **111**, 411–419 (2002).
[25]S. Hou, K. Solna, and H. Zhao, "Imaging of location and geometry for extended targets using the response matrix," J. Comput. Phys. **199**, 317–338 (2004).
[26]H. Zhao, "Analysis of the response matrix for an extended target," SIAM J. Appl. Math. **64**, 725–745 (2004).
[27]J.-P. Berenger, "A perfectly matched layer for the absorption of electromagnetic waves," J. Comput. Phys. **114**, 185–200 (1994).
[28]D. Colton and R. Kress, *Inverse Acoustic and Electromagnetic Scattering Theory*, 2nd ed. (Springer, Berlin, 1998).